Letters

Study of Charging Current Ripple Suppression for Battery Energy Storage Converter Under Distorted Grid Voltages

Haoqing Cai, *Student Member, IEEE*, Min Chen, *Senior Member, IEEE*, Changsheng Hu, *Senior Member, IEEE*, and Sheng Ren, *Student Member, IEEE*

***Abstract*—This letter proposes a charging current ripple suppression strategy for battery energy storage T-type three-level converter. Under distorted grid voltage scenarios, the harmonic contents of grid voltage lead to current ripple during battery charging. Theoretical analysis and mathematical derivations of the charging current ripple are presented. Based on the analysis, a control scheme for suppressing the charging current ripple is proposed by simplified calculating to obtain the amplitude and phase of harmonic reference current, and adding a charging current suppression loop. The suppression performance is verified via a 100-kW three-phase three-wire T-type three-level converter with battery. The experimental results prove that the charging current ripple can be effectively eliminated with the proposed strategy.**

***Index Terms*—Charging current ripple, distorted grid voltages, harmonic current, three-phase three-wire T-type three-level converter.**

I. Introduction

RECENTLY, due to the development of renewable energy and the growing global attention to the energy crisis, battery energy storage system (BESS) has attracted widespread attention. Generally, BESS is composed of three parts, i.e., batteries for storing energy, battery management system for monitoring battery packs, and power conversion system for transferring energy between batteries and the power grid [1].

In a three-phase system, the second harmonic current ripple tends to appear in the battery cell, which causes additional loss and accelerates battery aging [2]. The manufacturers often recommend a current ripple of less than 5% of the rated amp-hour capacity [2], [3]. Therefore, various researches have been conducted on the suppression of the current ripple at twice the fundamental frequency [2], [4], [5], [6]. Passive notch filters composed of *L-C* resonant circuits can be tuned at twice the fundamental frequency to shunt the second-order battery current ripple [4]. But this method involves large passive components, which increases the system volume and cost. Active filters, which generally insert a dc–dc converter to control the second-order ripple actively can also achieve low-frequency ripple-free current [5], and the demand for large passive components is reduced but not avoided because the second ripple has to be absorbed.

However, with the growing application of power electronic converters incorporated into the grid, the grid tends to incur harmonic distortion, which can lead to other low-frequency current ripples. Some literature focused on the impact of distorted grid voltages on torque ripple in doubly fed induction generator (DFIG) applications [6], [7], [8], [9]. Proportional integral (PI) regulator and resonant controller are employed to eliminate torque oscillations in DFIG under distorted grid voltages [6], [7]. Furthermore, second-order generalized integrator [8] and high-order generalized integrator [9] are applied for wind-solar systems to minimize torque and grid active power ripple under the unbalanced and distorted grid. While in BESS, the negative effect on battery under distorted grid voltages still lacks a profound study. For single-stage three-phase three-wire T-type three-level converter, the methods introduced in [4] and [5] can be similarly adopted but inevitably require additional hardware implementation. Neutral point clamped voltage source converter under the distorted grid has been studied [10], [11]. Reference current can be calculated according to instantaneous power analysis and the harmonic currents are controlled by reduced-order generalized integrator, contributing to power filtering [10]. But resonant controllers may face stability challenges. Model predictive control without phase-locked loop is proposed in [11], which generates flexible reference current by using a tuning parameter to reduce the active power oscillation flexibly under the distorted grid. Nevertheless, the calculation burden is relatively high. Moreover, in [10] and [11], the mathematical model and experimental validation of battery charging current ripple are not presented.

In view of the current ripple induced by the harmonic contents of distorted grid voltages, this letter proposes a charging current ripple suppression strategy without additional hardware cost for three-phase converters. The proposed strategy is based on the idea of simplified calculating to obtain the amplitude and

Manuscript received 30 November 2022; revised 9 February 2023 and 8 March 2023; accepted 23 March 2023. Date of publication 29 March 2023; date of current version 19 May 2023. This work was supported by the National Natural Science Foundation of China under Grant 52037010. *(Corresponding authors: Min Chen; Changsheng Hu.)*

The authors are with the College of Electrical Engineering, Institute of Power Electronics, Zhejiang University, Hangzhou 310027, China (e-mail: ee_hqcai@zju.edu.cn; heaven@zju.edu.cn; hucs@zju.edu.cn; rensheng_173@foxmail.com).

Color versions of one or more figures in this article are available at https://doi.org/10.1109/TPEL.2023.3262946.

Digital Object Identifier 10.1109/TPEL.2023.3262946

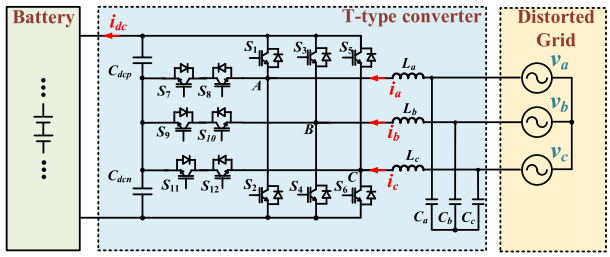

Fig. 1. Diagram of three-phase three-wire T-type three-level converter based power conversion system under distorted grid voltages.

phase of harmonic reference current for suppressing the charging current ripple, and adding a three-phase harmonic modulation control loop with the information of the calculated reference current phase and the PI control of the calculated reference current amplitude. Fifth, seventh, and 11th harmonic voltage extraction blocks for the grid and fifth, seventh, and 11th current extraction blocks for output inductors help the calculation.

In this letter, the theoretical analysis and mathematical derivations under distorted grid voltages are presented in Section II. With the mechanism of current ripple generation, the proposed control scheme and the theoretical suppression effectiveness are introduced in Section III. Finally, in Section IV, experimental results based on a 100-kW three-phase three-wire T-type three-level converter with battery are presented to verify the effectiveness of the strategy.

The T-type three-level converter is taken as an example in this letter. The proposed control strategy is also suitable for other three-phase voltage-source converters.

II. Analysis of Charging Current Ripple Under Distorted Grid Voltages

The diagram of a power conversion system based on a three-phase three-wire T-type three-level converter is presented in Fig. 1. v_a, v_b, and v_c are three-phase grid voltages. i_a, i_b, and i_c are three-phase inductor currents. $i_{\rm dc}$ is the battery charging current. L_a, L_b, and L_c are three-phase filter inductors. The inductance of L_a, L_b, and L_c is L. During battery charging, the power is converted from the grid to the battery.

Considering the grid voltage distortion, the charging current ripple will appear due to the reason analyzed as follows.

Supposing the following conditions are satisfied.

1) Three-phase grid voltages are balanced.
2) Power factor is equal to 1 during battery charging.
3) Harmonic distortion cannot be ignored.

Fifth, seventh, and 11th harmonic contents are mainly considered in the following analysis. The three-phase grid voltage and three-phase inductor current are expressed as, (1) and (2) shown at the bottom of the next page, where V_1, V_5, V_7, and V_{11} are the amplitudes of the fundamental, fifth, seventh, and 11th harmonic grid voltage, respectively. I_1, I_5, I_7, and I_{11} are the amplitudes of the fundamental, fifth, seventh, and 11th harmonic current, respectively.

In order to obtain the voltage at the converter side $v'_a(t)$, $v'_b(t)$, $v'_c(t)$, the impedance of the inductor is taken into consideration. As shown in Fig. 2, the simplified circuit of phase a is taken as an example. $v'_a(t)$ is the total voltage at the converter side. $v'_{a1}(t)$, $v'_{a5}(t)$, $v'_{a7}(t)$, and $v'_{a11}(t)$ are fundamental, fifth, seventh, and 11th harmonic voltage at the converter side, respectively.

The relationship between voltage at the converter side and the grid side is obtained as

$$\begin{bmatrix} v'_a(t) \\ v'_b(t) \\ v'_c(t) \end{bmatrix} = \begin{bmatrix} v_a(t) \\ v_b(t) \\ v_c(t) \end{bmatrix} - L\frac{d}{dt}\begin{bmatrix} i_a(t) \\ i_b(t) \\ i_c(t) \end{bmatrix}. \tag{3}$$

Assuming the battery voltage is $V_{\rm battery}$, the battery current can be calculated as

$$i_{\rm dc}(t) = \frac{1}{V_{\rm battery}}\begin{bmatrix} v'_a(t) & v'_b(t) & v'_c(t) \end{bmatrix}\begin{bmatrix} i_a(t) \\ i_b(t) \\ i_c(t) \end{bmatrix}. \tag{4}$$

Combining (1), (2), (3), (4) and ignoring the small items, the battery current $i_{\rm dc}(t)$ is derived as

$$\begin{aligned} i_{\rm dc}(t) = \frac{1}{V_{\rm battery}}\Bigg[&\frac{3}{2}V_1I_1 + \frac{3}{2}(V_5+V_7)I_1\cos(6\omega t) \\ &+ \frac{3}{2}V_{11}I_1\cos(12\omega t) \\ &+ (I_5+I_7)\sqrt{\left(\frac{3}{2}V_1\right)^2 + (9\omega L I_1)^2}\cos(6\omega t - \alpha_1) \\ &+ I_{11}\sqrt{\left(\frac{3}{2}V_1\right)^2 + (18\omega L I_1)^2}\cos(12\omega t - \alpha_2)\Bigg] \end{aligned} \tag{5}$$

where

$$\begin{cases} \alpha_1 = \arctan\left(\frac{6\omega L I_1}{V_1}\right) \\ \alpha_2 = \arctan\left(\frac{12\omega L I_1}{V_1}\right). \end{cases} \tag{6}$$

According to (5) and (6), the battery will suffer from sixth and 12th charging current ripple caused by the fifth, seventh, and 11th harmonic contents of the grid voltage. Considering a three-phase system: the operating power is 100 kW. The rms value of the fundamental grid voltage is 235 V. The rms value of fifth, seventh, and 11th harmonic grid voltages are 13.5, 3.8, and 3.2 V, respectively. The charging current $i_{\rm dc}(t)$ and line voltage $v_{ab}(t)$ in a fundamental cycle T_s are shown in Fig. 3(a).

III. Proposed Charging Current Ripple Suppression Strategy for T-Type Three-Level Converter

To effectively suppress the charging current ripple, the amplitude and phase of fifth, seventh, and 11th harmonic currents are selected as controlling variables. The proposed strategy is based on the idea of simplified calculating to obtain the amplitude and phase of harmonic reference current for suppressing the charging current ripple, and adding a three-phase harmonic modulation control loop with the information of the calculated reference current phase and the PI control of the calculated reference current amplitude. Fifth, seventh, and 11th harmonic voltage extraction blocks for the grid and fifth, seventh, and 11th

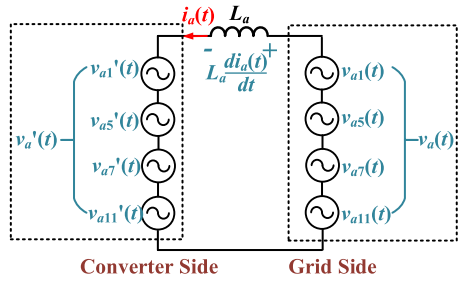

Fig. 2. Simplified equivalent circuit of the interaction between the converter and power grid with fifth, seventh, and 11th harmonic distortion (phase *a*).

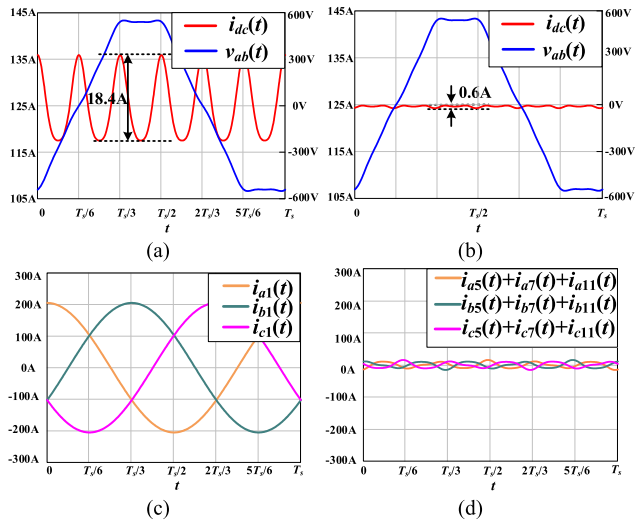

Fig. 3. Theoretical waveform. (a) Charging current $i_{\rm dc}(t)$ and line voltage without current ripple suppression control. (b) Charging current $i_{\rm dc}(t)$ and line voltage with current ripple suppression control. (c) Fundamental current $i_{a1}(t)$, $i_{b1}(t)$, and $i_{c1}(t)$. (d) Injected harmonic current with current ripple suppression control.

harmonic current extraction blocks for output inductors help the calculation.

The charging current with the controlled fifth, seventh, and 11th harmonic currents is expressed as

$$i_{\rm dc}(t)=\frac{1}{V_{\rm battery}}\left[\frac{3}{2}V_1I_1+\frac{3}{2}(V_5+V_7)I_1\cos(6\omega t)+\frac{3}{2}V_{11}I_1\cos(12\omega t)\right.$$
$$+I_5'\sqrt{\left(\frac{3}{2}V_1\right)^2+(9\omega LI_1)^2}\cos\left(6\omega t+\varphi^{(5)}-\alpha_1\right)$$
$$+I_7'\sqrt{\left(\frac{3}{2}V_1\right)^2+(9\omega LI_1)^2}\cos\left(6\omega t+\varphi^{(7)}-\alpha_1\right)$$
$$+I_{11}'\sqrt{\left(\frac{3}{2}V_1\right)^2+(18\omega LI_1)^2}$$
$$\left.\times\cos\left(12\omega t+\varphi^{(11)}-\alpha_2\right)\right] \tag{7}$$

where I_5', I_7', and I_{11}' are the controlled amplitudes of the fifth, seventh, and 11th harmonic currents, respectively. $\varphi^{(5)}$, $\varphi^{(7)}$, and $\varphi^{(11)}$ are the phase angles of the fifth, seventh, and 11th harmonic current leading to the fifth, seventh, and 11th harmonic voltage, respectively.

The amplitude and phase of fifth, seventh, and 11th harmonic currents are controlled as

$$\begin{cases} I_5'=-\dfrac{V_5I_1}{\sqrt{(V_1)^2+(6\omega LI_1)^2}} \\ \varphi^{(5)}=\arctan\left(\dfrac{6\omega LI_1}{V_1}\right)\end{cases} \tag{8}$$

$$\begin{cases} I_7'=-\dfrac{V_7I_1}{\sqrt{(V_1)^2+(6\omega LI_1)^2}} \\ \varphi^{(7)}=\arctan\left(\dfrac{6\omega LI_1}{V_1}\right)\end{cases} \tag{9}$$

$$\begin{cases} I_{11}'=-\dfrac{V_{11}I_1}{\sqrt{(V_1)^2+(12\omega LI_1)^2}} \\ \varphi^{(11)}=\arctan\left(\dfrac{12\omega LI_1}{V_1}\right).\end{cases} \tag{10}$$

When (8), (9), and (10) are applied, the theoretical waveform of the charging current $i_{\rm dc}(t)$ and line voltage $v_{ab}(t)$ in a fundamental cycle T_s are shown in Fig. 3(b). Fig. 3(a) is plotted by (5), while Fig. 3(b) is plotted by (7), (8), (9), and (10). It can be seen that the peak–peak value of the current ripple is eliminated from 18.4 to 0.6 A. The fundamental current $i_{a1}(t)$, $i_{b1}(t)$, and $i_{c1}(t)$ are shown in Fig. 3(c). The injected harmonic current with the proposed current ripple suppression control is shown in Fig. 3(d). The charging current ripple caused by the harmonic grid voltages can be mitigated.

In practice, for simpler implementation, the term $6\omega LI_1$ in amplitude calculation can be ignored, for it is generally much less than fundamental voltage, especially at low charging power. The calculation of phase angle φ can be approximated by Taylor's theorem.

$$\begin{bmatrix} v_a(t)\\ v_b(t)\\ v_c(t)\end{bmatrix}=\begin{bmatrix} \cos(\omega t) & \cos(5\omega t) & \cos(7\omega t) & \cos(11\omega t)\\ \cos(\omega t-\frac{2}{3}\pi) & \cos(5\omega t+\frac{2}{3}\pi) & \cos(7\omega t-\frac{2}{3}\pi) & \cos(11\omega t+\frac{2}{3}\pi)\\ \cos(\omega t+\frac{2}{3}\pi) & \cos(5\omega t-\frac{2}{3}\pi) & \cos(7\omega t+\frac{2}{3}\pi) & \cos(11\omega t-\frac{2}{3}\pi)\end{bmatrix}\begin{bmatrix} V_1\\ V_5\\ V_7\\ V_{11}\end{bmatrix} \tag{1}$$

$$\begin{bmatrix} i_a(t)\\ i_b(t)\\ i_c(t)\end{bmatrix}=\begin{bmatrix} \cos(\omega t) & \cos(5\omega t) & \cos(7\omega t) & \cos(11\omega t)\\ \cos(\omega t-\frac{2}{3}\pi) & \cos(5\omega t+\frac{2}{3}\pi) & \cos(7\omega t-\frac{2}{3}\pi) & \cos(11\omega t+\frac{2}{3}\pi)\\ \cos(\omega t+\frac{2}{3}\pi) & \cos(5\omega t-\frac{2}{3}\pi) & \cos(7\omega t+\frac{2}{3}\pi) & \cos(11\omega t-\frac{2}{3}\pi)\end{bmatrix}\begin{bmatrix} I_1\\ I_5\\ I_7\\ I_{11}\end{bmatrix} \tag{2}$$

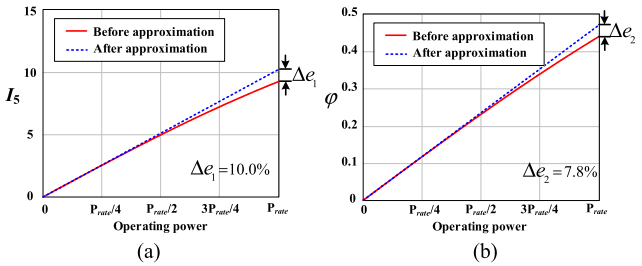

Fig. 4. Comparison of approximated calculation. (a) For amplitude. (b) For phase.

Taking fifth harmonic content as an example, (11) is obtained from (8) as a simpler form to be implemented

$$\begin{cases} I_5' = -\frac{V_5 I_1}{V_1} \\ \varphi^{(5)} = \frac{6\omega L I_1}{V_1}. \end{cases} \tag{11}$$

The impact of approximation on amplitude and phase are shown in Fig. 4(a) and (b). Below 50% rated power, the two curves are almost the same for both amplitude and phase. While above 50% rated power, the approximation error increases along with the operating power. The maximum approximation error appears at rated power, where the errors of amplitude and phase are $\Delta e_1 = 10.0\%$ and $\Delta e_2 = 7.8\%$, respectively.

Take the abovementioned case as an example. When fifth, seventh, and 11th references are all approximated, the peak–peak value of the current ripple with the approximated calculation is 2.4 A at 100 kW.

To achieve the control goal of (8), (9), and (10), a control scheme by adding a harmonic extraction block and a three-phase harmonic modulation control loop is proposed, as shown in Fig. 5.

Using Park Transformation with constant amplitude, the V_1, V_5, V_7, V_{11}, I_1, I_5', I_7', and I_{11}' in (7) can be corresponding to $v_d^{(1)}$, $v_d^{(5)}$, $v_d^{(7)}$, $v_d^{(11)}$, $i_d^{(1)}$, $i_d^{(5)}$, $i_d^{(7)}$, and $i_d^{(11)}$ in Fig. 5, respectively.

The added harmonic extraction block is composed of the extraction of harmonic voltage and current. For fifth harmonic voltage, Inverse Park Transformation is used to transform voltages $v_d^{(1)}$ and $v_q^{(1)}$ from the fundamental dq synchronous frame to abc stationary frame $v_a^{(1)}, v_b^{(1)}$, and $v_c^{(1)}$. v_{ah}, v_{bh}, and v_{ch} are the subtraction of the sampled three-phase voltages v_a, v_b, v_c, and fundamental voltages $v_a^{(1)}, v_b^{(1)}, v_c^{(1)}$. With the phase angle of -5θ, v_{ah}, v_{bh}, and v_{ch} are transformed into the fifth dq synchronous frame $v_d^{(5)}$ and $v_q^{(5)}$. The extraction is similar for seventh and 11th harmonic voltages. The same process is adopted for harmonic current extraction.

For the three-phase harmonic modulation control loop, $v_d^{(1)}, v_d^{(5)}$, and $i_d^{(1)}$ are used for the calculation of fifth harmonic reference current. Under the fifth dq synchronous frame, the fifth d-axis harmonic current is controlled to the fifth d-axis reference current $I_{dref}^{(5)}$ by a PI controller. The fifth q-axis harmonic current is controlled to 0 by a PI controller. The outputs of the above two PI controllers are the fifth modulation waves in the fifth dq synchronous frame. The calculated phase angle $\varphi^{(5)}$ is compensated to the angle used in the fifth Park

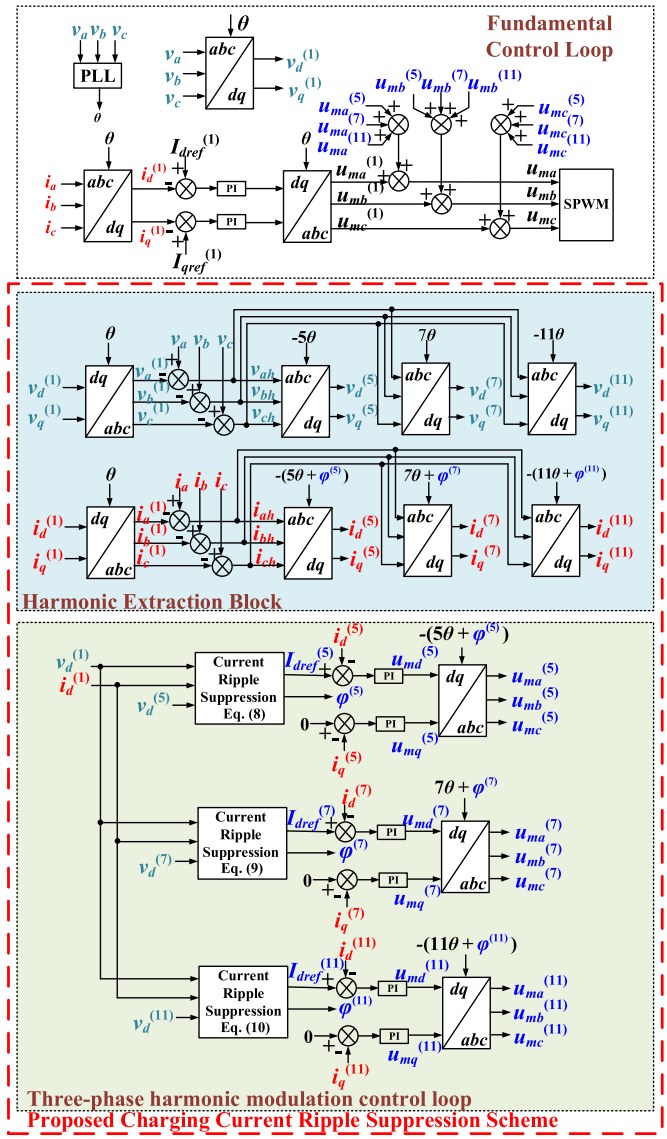

Fig. 5. Overall control scheme of the proposed charging current ripple suppression strategy.

Transformation for harmonic current extraction and the fifth Inverse Park Transformation for the fifth modulation wave. The fifth modulation waves $u_{ma}^{(5)}$, $u_{mb}^{(5)}$, and $u_{mc}^{(5)}$ obtained by the fifth Inverse Transformation are added to the fundamental modulation waves $u_{ma}^{(1)}$, $u_{mb}^{(1)}$, and $u_{mc}^{(1)}$. The obtained harmonic modulation voltages $u_{ma}^{(7)}, u_{mb}^{(7)}, u_{mc}^{(7)}, u_{ma}^{(11)}, u_{mb}^{(11)}$, and $u_{mc}^{(11)}$ are also added to the fundamental modulation waves similarly. In this way, the final modulation waves are obtained as u_{ma}, u_{mb}, and u_{mc}.

Although the proposed strategy helps depress the battery charging current ripple, it will inevitably affect the quality of the output current. According to IEEE std. 519-2022 [12], the harmonic current limits are as follows.

1) The individual harmonic distortion (2nd–11th) should be lower than 4.0%.
2) The total Demand distortion should be lower than 5.0%.

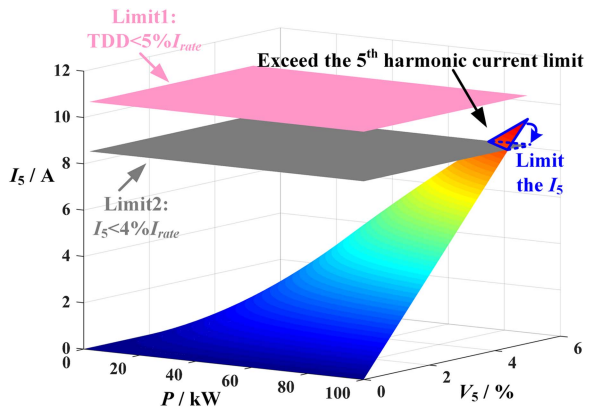

Fig. 6. Three-dimensional surface plot of injected fifth harmonic current and the IEEE standard 519-2022 for harmonic current.

TABLE I
PARAMETERS FOR THREE-PHASE THREE-WIRE T-TYPE THREE-LEVEL CONVERTER AND BATTERY

Parameter	Symbol	Value
Rated power	P_e	100 kW
Grid phase voltage (rms)	v_a, v_b, v_c	230 V
Grid frequency	f	50 Hz
Upper and lower dc bus capacitor	C_{dcp}, C_{dcn}	11 mF
Filter inductor	L_a, L_b, L_c	380 μH
Switching frequency	f_s	10 kHz
Battery Voltage	$V_{battery}$	800 V

Considering the main injected harmonic current is fifth harmonic current, the amplitude of the fifth harmonic current and the standard limits are plotted in a three-dimensional surface, as shown in Fig. 6. It can be seen from Fig. 6 that the fifth harmonic current and THD are higher when the operating power is higher and the grid is more distorted. Once the calculated amplitude exceeds the standard limits, the amplitude of the fifth harmonic current has to be limited to meet the requirements. For example, the amplitude of the injected fifth harmonic current must be limited to less than 8.6 A for a 100-kW converter.

IV. EXPERIMENTAL RESULTS

An experimental platform composed of a 100-kW three-phase three-wire T-type three-level converter and a lithium battery is built for verification. The control scheme is implemented with a TMS320F2808 DSP and the parameters of the experiment are listed in Table I.

The fifth harmonic voltage is apparently higher than other higher harmonics generally [13], [14]. Table II lists the harmonic conditions of one of the actual power grids for the test measured by YOKOGAWA WT1800. For simplification, the fifth and seventh harmonics are mainly considered to suppress the current ripple in the experiment.

Fig. 7 shows the battery charging current ripple suppression effect at 50 kW (50% rated power). In Fig. 7(a) and (b), $i_{\rm dc}$ represents the waveform of the charging current measured at the battery side. v_{ab} is the line voltage of phase a and phase b. For more clear observation, the amplitude zoom of $i_{\rm dc}$ is also displayed. It can be seen from Fig. 7 that the charging current ripple, which is injected into the battery, is obvious with the original control strategy, but once the proposed scheme is adopted, the measured current ripple is reduced from 7.9 to 3.5 A.

Fig. 8 shows the battery charging current ripple suppression effect at 100 kW (rated power). The definitions of symbols are the same as in Fig. 7. It can be seen from Fig. 8 that the battery charging current is reduced from 13.2 to 5.7 A when the proposed charging current suppression strategy is adopted.

For clearer observation of charging current ripple contents, harmonic spectrums of the charging current ripple in Figs. 7 and 8 are displayed in Figs. 9 and 10. Fig. 9 compares the harmonic

TABLE II
HARMONIC CONTENTS OF GRID VOLTAGES IN THE EXPERIMENT

Harmonic order	Phase a	Phase b	Phase c
1	235.69 V, 100%	236.48 V, 100%	235.14 V, 100%
2	0.05 V, 0.021%	0.04 V, 0.018%	0.03 V, 0.012%
3	0.77 V, 0.326%	0.64 V, 0.273%	0.30 V, 0.129%
4	0.04 V, 0.016%	0.05 V, 0.022%	0.04 V, 0.017%
5	13.35 V, 5.665%	13.60 V, 5.751%	13.86 V, 5.896%
6	0.07 V, 0.029%	0.02 V, 0.008%	0.06 V, 0.024%
7	3.71 V, 1.576%	3.3 7V, 1.427%	3.83 V, 1.628%
8	0.03 V, 0.011%	0.06 V, 0.025%	0.04 V, 0.018%
9	0.45 V, 0.191%	0.16 V, 0.067%	0.56 V, 0.239%
10	0.03 V, 0.012%	0.06 V, 0.027%	0.07 V, 0.028%
11	3.30 V, 1.398%	3.22 V, 1.362%	3.51 V, 1.492%

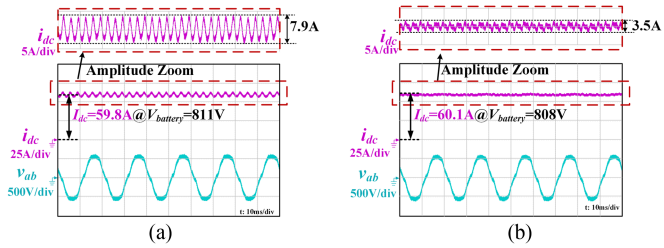

Fig. 7. Waveform of charging current ripple suppression effect at 50 kW (50% rated power). (a) Original control strategy. (b) Proposed charging current suppression strategy.

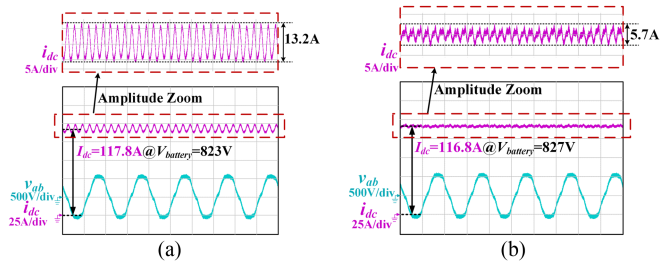

Fig. 8. Waveform of charging current ripple suppression effect at 100 kW (rated power). (a) Original control strategy. (b) Proposed charging current suppression strategy.

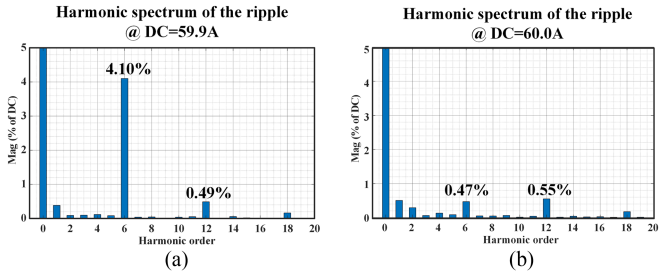

Fig. 9. Harmonic spectrum of charging current ripple at 50 kW (50% rated power). (a) Original control strategy. (b) Proposed charging current ripple suppression strategy.

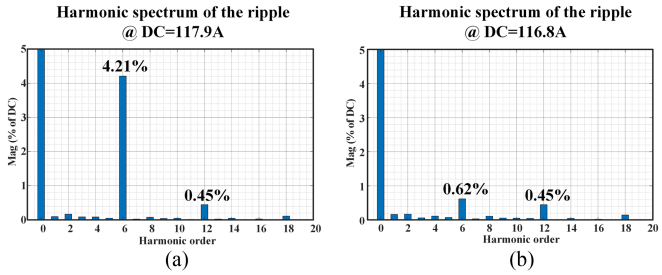

Fig. 10. Harmonic spectrum of charging current ripple at 100 kW (rated power). (a) Original control strategy. (b) Proposed charging current ripple suppression strategy.

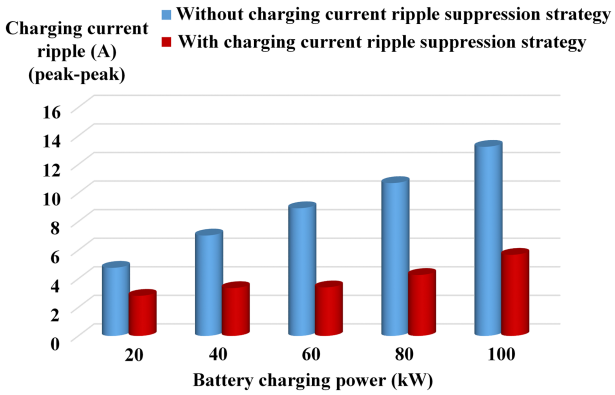

Fig. 11. Charging current ripple suppression effect at different charging power.

contents of the original control strategy and the proposed scheme at 50 kW. The sixth harmonic content of the current ripple decreases from 4.10% to 0.47%. In Fig. 10, the sixth harmonic content of the current ripple is eliminated from 4.21% to 0.62% at 100 kW. It can be concluded that the current ripple caused by the distorted grid has been significantly depressed to a low level.

Fig. 11 shows the battery charging current ripple suppression effect with the proposed strategy at different charging power. It reveals that when the load becomes heavier, the battery charging current ripple also increases. Besides, it can be concluded that the proposed strategy can effectively suppress the battery charging current from light to full load under distorted grid voltages.

From the experimental results, the charging current ripple is not completely suppressed due to the reasons listed below. First, the current ripple is composed of other low harmonic contents, as shown in Figs. 9 and 10. Second, the approximation of calculation and detecting error will affect the ripple suppression performance. Finally, the sinusoidal modulation method for the three-phase T-type converter leads to a second content in the duty ratio of the horizontal switches. This brings up a third harmonic in the neutral point current and voltage, and it will cause another part of the sixth current ripple, which is not influenced by the distorted grid.

V. Conclusion

A battery charging current ripple suppression strategy for battery energy storage T-type three-level converter under distorted grid voltages is proposed in this letter. The proposed control strategy adopts simplified calculation to obtain the amplitude and phase of the harmonic reference current, and adds a three-phase harmonic modulation control loop with the information of the calculated reference current amplitude and phase. Theoretical analysis and mathematical equations are presented for the charging current ripple. Based on the analysis, the proposed control scheme is introduced. With the proposed method, the charging current ripple can be effectively suppressed without additional hardware circuits. Finally, the experimental results on a 100-kW three-phase three-wire T-type three-level converter with a lithium battery demonstrate the feasibility of the proposed strategy.

References

[1] H. Qian, J. Zhang, J. -S. Lai, and W. Yu, "A high-efficiency grid-tie battery energy storage system," *IEEE Trans. Power Electron.*, vol. 26, no. 3, pp. 886–896, Mar. 2011.

[2] Z. Li, R. Lizana, S. M. Lukic, A. V. Peterchev, and S. M. Goetz, "Current injection methods for ripple-current suppression in delta-configured split-battery energy storage," *IEEE Trans. Power Electron.*, vol. 34, no. 8, pp. 7411–7421, Aug. 2019.

[3] Emerson Network Power, "Effects of ac ripple current on VRLA battery life," . Accessed: Apr. 1, 2023. [Online]. Available: https://datacsi.com/wp-content/uploads/white-papers/Effects-of-AC-Ripple-Current-on-VRLA-Battery-Life-Technical-Note-TN-00008.pdf

[4] X. Zhou, X. Yu, S. Lukic, and A. Huang, "LCL filter utilized in battery charging applications to achieve compact size and low ripple charging," in *Proc. IEEE Energy Convers. Congr. Expo.*, 2012, pp. 660–665.

[5] X. Liu, H. Li, and Z. Wang, "A fuel cell power conditioning system with low-frequency ripple-free input current using a control-oriented power pulsation decoupling strategy," *IEEE Trans. Power Electron.*, vol. 29, no. 1, pp. 159–169, Jan. 2014.

[6] H. Xu, J. Hu, and Y. He, "Operation of wind-turbine-driven DFIG systems under distorted grid voltage conditions: Analysis and experimental validations," *IEEE Trans. Power Electron.*, vol. 27, no. 5, pp. 2354–2366, May 2012.

[7] J. Hu, H. Xu, and Y. He, "Coordinated control of DFIG's RSC and GSC under generalized unbalanced and distorted grid voltage conditions," *IEEE Trans. Ind. Electron.*, vol. 60, no. 7, pp. 2808–2819, Jul. 2013.

[8] S. Das and B. Singh, "Flexible ripple minimization technique for wind-solar renewable energy system under unbalanced and distorted grid conditions," *IEEE Trans. Ind. Appl.*, vol. 58, no. 5, pp. 6739–6751, Sep./Oct. 2022.

[9] S. Das and B. Singh, "Multi-objective control strategy for power quality improvement in wind-solar distributed generation system under harmonically distorted grid," *IEEE Trans. Ind. Appl.*, vol. 58, no. 5, pp. 5697–5710, Sep./Oct. 2022.

[10] J. Moriano, M. Rizo, E. J. Bueno, R. Martin, and F. J. Rodriguez, "A novel multifrequency current reference calculation to mitigate active power fluctuations," *IEEE Trans. Ind. Electron.*, vol. 65, no. 1, pp. 810–818, Jan. 2018.

[11] S. R. Mohapatra and V. Agarwal, "Model predictive control for flexible reduction of active power oscillation in grid-tied multilevel inverters under unbalanced and distorted microgrid conditions," *IEEE Trans. Ind. Appl.*, vol. 56, no. 2, pp. 1107–1115, Mar./Apr. 2020.

[12] *IEEE Standard for Harmonic Control in Electric Power Systems*, IEEE Standard 519-2022, (Revision IEEE Std 519-2014), pp. 1–31, Aug. 2022, doi: 10.1109/IEEESTD.2022.9848440.

[13] J. P. Nelson, "A better understanding of harmonic distortion in the petrochemical industry," *IEEE Trans. Ind. Appl.*, vol. 40, no. 1, pp. 220–231, Jan./Feb. 2004.

[14] M. Yazdani-Asrami, S. M. B. Sadati, and E. Samadaei, "Harmonic study for MDF industries: A case study," in *Proc. IEEE Appl. Power Electron. Colloq.*, 2011, pp. 149–154.